ANALYSIS OF THE IMPACT PROCESS AT DIKES WITH CROWN WALLS AND PARAPETS

Giuseppina Palma[1], Sara Mizar Formentin[1] and Barbara Zanuttigh[1]

This paper is focused on the analysis of the impact process at dikes with crown walls and parapets under breaking and non-breaking waves. A small-scale laboratory campaign was performed at the Hydraulic Laboratory of Bologna. The experiments were aimed to analyze the vertical pressure distribution along the crown wall and the resulting wave forces, by varying geometrical and hydraulic parameters. The tested configurations included different off-shore slopes, dike crest widths, crown-wall heights, dike crest freeboards and the inclusion of the parapet. The measurements were combined with the image analysis of the run-up and of the wave impact process. A sub-set of the experiments was numerically reproduced, with the openFOAM modelling suite, to support and to extend the experimental results. The results confirmed the link between the air content, the shape and the magnitude of the pressures according to the breaker type, already observed for larger-scale experiments.

Keywords: dike, pressure, wave loads, crown wall, parapet, breaking wave, non-breaking wave, numerical modelling, image analysis

INTRODUCTION

A promising solution to upgrade coastal and harbour defense structures, to face the effects of climate change, is represented by the use of crown walls (Burcharth et al., 2014), eventually with parapets (Van Doorslaer et al., 2015; Formentin and Zanuttigh, 2019). While a wide literature is available on the combined effects of the wave breaking and of the air entrapment on the wave impacts at seawalls (Plumerault et al., 2012), few works are dedicated to dike-type structures with crown walls. Martinelli et al. (2018) and Castellino et al. (2018) performed small-scale experiments and numerical modelling to evaluate the effect on the vertical pressure distributions of parapets placed on top of vertical walls under *non-breaking* waves. The results showed that the inclusion of the parapet increases the pressures along the crown wall due to the impulsive pressures enhanced by the confined return flow. Van Dooslaer et al. (2015, 2017) and De Finis et al. (2020) confirmed the same result in case of parapets on the crown walls of smooth dikes. Their research was primarily focused on the reduction rate of the overtopping discharge at the rear side of the structure, under *non-breaking* waves only. Later, Zanuttigh and Formentin (2018) extended this database by testing similar structures also under *breaking* waves. The gathered data are here used to calibrate a numerical model, developed in the openFOAM environment, aimed to support and extend the laboratory investigations. Indeed, the reliability of numerical models in representing the wave impact dynamics, and the so the wave forces acting against the crown walls, was deeply investigated (Ma et al., 2014; Liu et al., 2019). However, these analyses were often focused on single and/or regular wave impacts, characterized by small air content.

Therefore, this paper aims at analyzing the effects of the air entrainment and of the model scale on the magnitude and on the distribution of the wave pressures at crown walls and parapets of smooth dikes, under both *breaking* and *non-breaking* waves. Specific objectives are i) to verify whether the findings by Bullock et al. (2007) for large-scale experiments are still valid at small model scale, and ii) to validate a reliable numerical model to support the physical investigation.

The paper is organized as follows. Section 2 presents the methodologies adopted, which implied both the physical and the numerical investigations. Section 3 describes the main results obtained during the laboratory campaign. Section 4 show the numerical model investigations, describing the calibration and the analysis of the wave impact, giving a qualitative indication about the air content associated to the tested breaker types.

METHODOLOGY

This work is based on the results of a new laboratory campaign on wave overtopping recently conducted at the University of Bologna. The new tests were aimed at collecting an extensive and systematic experience on the wave impacts at crown walls with and without parapets. The analysis of the pressures acting against the structure is supported by image analysis to derive the link between the air content, the magnitude of the loads and the shape of the pressure signals. The numerical model, developed in the openFOAM environment, was calibrated based on the experimental work, to correctly

[1] DICAM, University of Bologna, V.le Risorgimento 2, Bologna, BO, 40136, Italy

reproduce the hydraulic and the structural performance of such structure, and to derive qualitative indications about the air content at the wave front.

Laboratory campaign

The laboratory campaign was performed at the Hydraulic Laboratory of the University of Bologna in the wave flume, that is 12 m long, 0.5 m wide and 1.0 m deep. It is provided by a piston wave-maker, capable of generating both regular and irregular wave attacks. The water depth h at the wave-maker should not exceed 0.4-0.45 m. The wave flume is provided with a recirculation system, composed by i) a recirculation conduit, ii) a pump and iii) a flowmeter, responsible of maintaining the water depth constant during the experiments. The characteristics of the wave conditions that can be implemented are: a maximum significant wave height H_s of approximately 0.06 m and a maximum wave length $L_{m-1,0}$ of ≈3 m. All the laboratory tests involved irregular wave series, characterized by a Jonswap spectrum with a peak enhancement factor γ=3.3. The tested wave conditions included wave heights H_s in the range of 0.05-0.06 m and spectral wave periods $T_{m-1,0}$ in the range of 0.85-1.45 s, giving two reference values of the wave steepness $s_{m-1,0}$≈0.03 or 0.04.

Several instruments were installed inside the wave flume and across the dike structure to measure the time series of the free-surface elevations and the pressures. Specifically, 3 resistive wave gauges (*wgs*), were placed at approximately 1.5·times the maximum $L_{m-1,0}$, to obtain information about the incident and reflected waves, according to Zelt & Skjelbreia (1992). A fourth *wg* was installed on the crest width to measure the thickness of the overtopping layer. All the *wgs* are characterized by a sample frequency of 100 Hz. To quantify the wave impacts, 3 pressure transducers were installed along the crown wall, characterized by: sample frequency of 1 kHz; range of measurement from 70 mbar to 700 mbar; accuracy of ±0.04% full scale; external diameter of 25 mm, internal diameter of 3 mm for the measurement of the pressures. The run-up and the wave impact processes were filmed by means of a full HD camera (30 fps) positioned outside the wave flume, in correspondence of the crest width. The full scheme of the wave flume, with reference to the position of the wave gauges, can be found in Zanuttigh & Formentin (2018).

The tested configurations consisted of smooth dikes with a crown wall at the inshore crest. The wall might include or not an inclined parapet. The layout of the typical cross-section, with reference to the main hydraulic and structural parameters, is given in Figure 1. Specifically, α is the constant dike offshore slope, G_c the crest width, h_w the height of the crown wall, ε the inclination of the parapet, and A_c and R_c the distance between the dike crest and the end of the crown wall from the still water level, respectively.

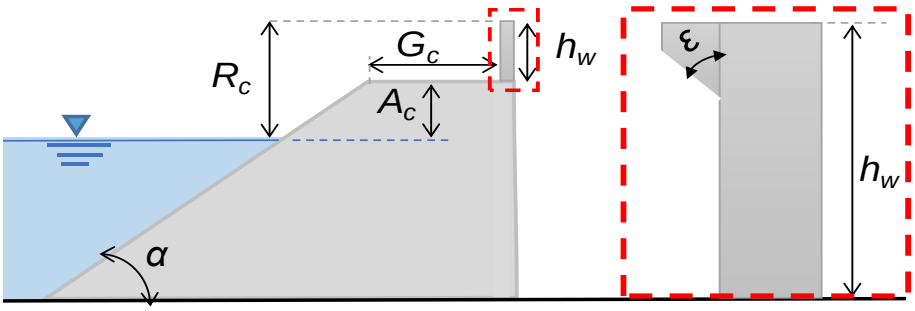

Figure 1. Cross-section of the investigated geometries.

The experiments were carried out in 1:20 scale and consisted of 128 irregular tests. The smooth slopes ($cot\alpha$=2 and 4) are characterized by different crest levels (A_c/H_s from 0 to 0.5) and crest widths (G_c=0.15 and 0.30 m). The combination of wall heights (h_w=0.04 and 0.05 m) and water levels (h) are such to determine relative freeboards R_c/H_s in the range 0.67-1.50. The angle of the parapet, when present, was fixed ε=30°, based on previous analyses (Zanuttigh & Formentin, 2018). The combination among the wave and the structure characteristics provide an Iribarren-Battjes breaker parameter $\xi_{m-1,0}$ in the range of 1.23 and 4.0, including in the database both *breaking* and *non-breaking* waves. Table 1 summarizes the tested wave conditions and geometries.

Table 1. Summary of the tested parameters during the laboratory campaign.		
A_c/H_s	**0**	**0.5**
H_s [m]	0.05; 0.06	0.05; 0.06
$s_{m-1,0}$ [-]	0.03; 0.04	0.03; 0.04
$cot(\alpha)$ [-]	2; 4	2; 4
G_c [-]	0.15; 0.30	0.15; 0.30
h_w [-]	0.04; 0.05	0.04; 0.05
parapet	no; yes	no; yes

Numerical investigation

The 2D numerical simulations were performed by means of a 2DV RANS-VOF software, i.e. openFOAM (OF). Specifically, the toolbox *waves2Foam*, originally developed at the Technical University of Denmark by Niels Gjøl Jacobsen et al. (2012), was used for the wave generation/absorption inside the numerical channel. It is a solver capable of solving 2 incompressible, isothermal immiscible fluids using the Volume Of Fluid (VOF) phase-fraction based interface capturing method. This library is a modification of the native solver *interFoam*, based on the Volume Average Reynolds Average Navier Stokes equations (VARANS). The fluids air and water are simultaneously tracked using the scalar field ϑ, which is equal to 0 for air and 1 for water. Intermediate values represent a mixture of the 2 fluids. In the momentum balance equation, an extra term is included to take into account of the surface tension between the 2 phases. The wave generation/absorption processes occurred by means of the application of the relaxation zone technique (active sponge layers), providing a large range of wave theories for both regular and irregular wave series.

The numerical simulations reproduced a sub-set of the laboratory wave conditions at the same laboratory scale. The irregular wave series, characterized by a Jonswap spectrum with a peak enhancement factor γ=3.3, are implemented by defining the values of H_s and T_p. The sub-set was selected to evaluate the variation of the forces acting on simple crown walls, under *breaking* and *non-breaking* waves, by varying the significant wave height H_s, the wave steepness $s_{m-1,0}$, and by keeping constant the crest width G_c and the height of the wall h_w. Table 2 summarizes the numerically tested parameters.

Table 2. Summary of the numerically tested parameters.		
A_c/H_s **[-]**	**0**	**0.5**
H_s [m]	0.05; 0.06	0.05; 0.06
$s_{m-1,0}$ [-]	0.03; 0.04	0.03; 0.04
$cot(\alpha)$ [-]	2; 4	2; 4
G_c [m]	0.30	0.30
h_w [m]	0.04	0.04

The length of the domain was set equal to 11.2 m, which corresponds to more than 3 times the wavelength L characterizing the tests (≈3 m). It was provided with an inlet relaxation zone for the wave generation, equal to 4.5 m, followed by 2 wavelengths to let the wave to be completely developed before reaching the structure. The position of the offshore edge of the crest with, and so of the crown wall, was kept constant for all the tests (10.7512 m and 11.0512 m, respectively-x coordinates). The dike footprint depends on the $cot\alpha$ values, and so on the length of the sloping part, i.e.1.72 m for $cot\alpha$=4 and 1.02 m for $cot\alpha$=2.

The numerical domain dimensions were set to correctly represent all the wave conditions. The mesh characteristics slightly change along the domain to minimize the computational effort, while maximizing the accuracy of the results. Specifically, the numerical domain was divided into 3 parts along the horizontal direction, with a cell size dimension of 0.05 m-0.002 m, 0.002 m and 0.002-0.02 m, respectively. The second zone is the one related to the run-up/wave impact processes. Therefore, a very refined constant grid was preferred. In the vertical direction, starting from the bottom, the cell size varies from 0.01 m to 0.002, in correspondence of the still water level, to reach the value of 0.05 m in correspondence of the atmosphere. The patches composing the numerical domain, which have to be characterized by a boundary condition for each initialized wave field, i.e. *alpha.water* (VOF), *p_rgh* (dynamic pressure), *U* (velocity), are summarized in Table 3.

Table 3. Boundary conditions implemented in the numerical model.

	alpha.water	p_rgh	U
Inlet	waveAlpha	zeroGradient	waveVelocity
Bottom	zeroGradient	zeroGradient	fixedValue
Outlet	fixedValue	zeroGradient	fixedValue
Atmosphere	inletOutlet	totalPressure	pressureInletOutletVelocity
Structure	zeroGradient	zeroGradient	fixedValue
frontBack	empty	Empty	empty

The numerical domain, shown in Figure 2, was equipped with 3 gauges, located in the same position of the laboratory wave flume, to measure the incident and the reflected waves (see Figure 2). In the numerical model, the number of the pressure transducers was increased by setting them every 0.005 m from the base of the crown wall, i.e. 9 numerical pressure transducers (see Figure 3). The average overtopping discharge rates q were computed by integrating the horizontal water velocity components (output every 0.005 m) along a virtual gauge placed at the rear side of the crown wall. Figure 3 shows a detailed scheme related to the pressures and the velocity-VOF outputs aim to quantify the forces F and the overtopping discharge rates q, respectively.

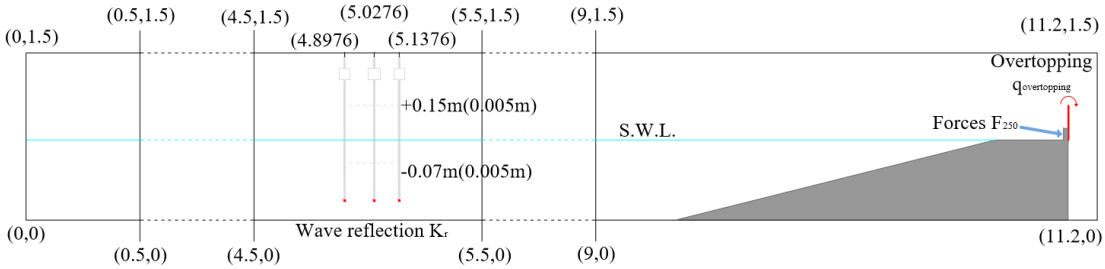

Figure 2. Scheme of the numerical domain, with reference to the virtual gauges and quantities measured.

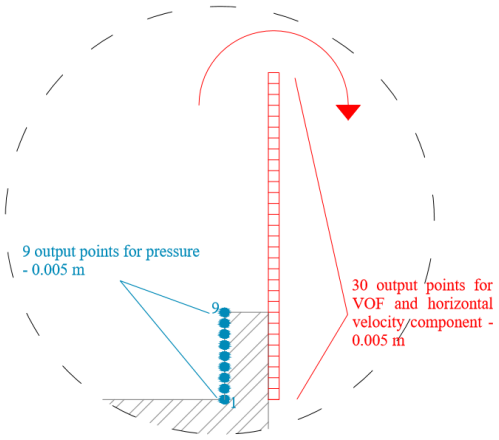

Figure 3. Scheme of the location of the pressure transducers and of the virtual gauge for the wave overtopping, in the numerical model.

LABORATORY ANALYSIS AND RESULTS

This Section presents the analysis performed on the laboratory campaign results. The results on the air entrainment derived from image visualization/analysis and on the reconstruction of the vertical profiles of the wave pressures from the transducers are in agreement with the literature available for large-scale experiments (Oumeraci et al., 1993; Bullock et al. 2007). Indeed, a strong correlation is found among the breaker types, the amount of air pockets entrapped and the type and the entity of the impact loads.

Image analysis and pressure signals

The literature presents different classifications methods of the wave impacts and the wave pressure signals, according to different aspects to be considered. Table 4 reports the classification of the tested wave conditions and the resulting pressure signals according to 3 of the most common methods: 1) the method based on the Iribarren-Battjes breaker parameter $\xi_{m-1,0}$, which classifies the pressure signals according to the nature of the wave breaking (surging, plunging, broken); 2) the method proposed by Oumeraci et al. (1993), aiming at characterizing the nature of wave impact (impact load, slightly breaking); 3) the method by Bullock et al. (2007), based on the air content associated to the wave impact (high aeration, low aeration).

Table 4. Classification and description of the tested wave conditions according to the breaker parameter, the type of the wave impact and the associated air content.

Breaker parameter (Iribarren-Battjes, 1973)	**Wave impact** (Oumeraci et al. 1993)	**Air content** (Bullock et al, 2007)
Surging (*non-breaking*, the wave front reaches the wall fully developed)	**Impact load**	**High-aeration** (*broken*, the wave front breaks against the wall)
Plunging (*slightly-breaking*, it represents a transition phase between the *non-breaking* and the *broken* wave	**Slightly breaking**	**Low-aeration** (*slightly-breaking*)

In this laboratory campaign, the wave impacts were classified according to the breaker type. Based on the values of $\xi_{m-1,0}$ calculated at the toe of the dike slope, the tested wave conditions involved: *surging* ($\xi_{m-1,0}$>2.0), *plunging* and *broken* ($\xi_{m-1,0}$<2.0) waves. The main difference is that the former breaks during the impact with the crown wall, while the latest two reach the structure during a transition phase (*plunging*/*slightly breaking*) or when they are already *broken*. Figure 4 shows a few frames of different wave impact types. In panel a), the *non-breaking* wave type reaches the crown wall before breaking; in panel b), the wave is breaking just at the end of the run-up process, overturning and hitting violently against the crest; the flow is characterized by the first air bubbles beneath the wave front. In panel c), the wave is already broken when completing the run-up process and when propagating along the crest width. The flow shows a high turbulence rates and huge air entrainment amount. In panel d), relative to the crest freeboard A_c=0, the wave is completely broken before reaching the top of the slope, and the flow along the crest is bore and low-energetic, due to the dissipation occurred during the wave run-up, presenting a significant level of air bubbles, which can be hardly individually detected. For all the tested conditions with A_c=0, the breaker types are always identified as *broken*; in case of A_c>0 instead, the breaker types can be either plunging (≈80-86%) or surging (≈7-10%) according to the value of $\xi_{m-1,0}$ associated to each incident wave.

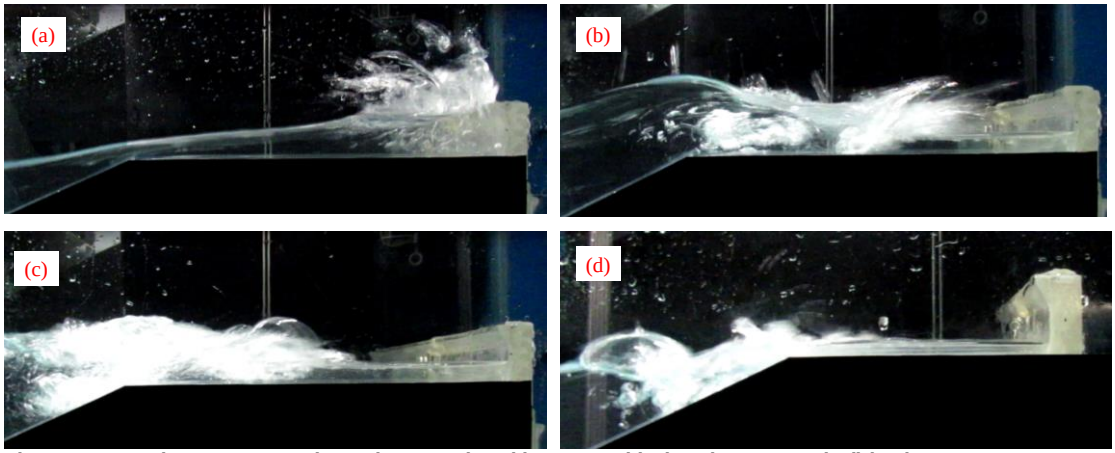

Figure 4. Wave impact types: a) surging, non-breaking wave; b) plunging wave; c), d) broken waves.

The Iribarren-Battjes classification, combined with the freeboard crest conditions, identified thus 3 wave types in the laboratory campaign. As an example, Figure 5 shows the signals associated to a *surging* (a), a *plunging* (b) and a *broken* wave (c) occurring consecutively during the same test (H_s=0.05 m, $s_{m-1,0}$=0.03 A_c/H_s=0, G_c=0.30 m, $cot\alpha$=2, h_w=0.5, ε=30°) at the pressure transducers P1 (in blue), P2 (in orange) and P3 (in yellow). By looking at these pressure signals obtained from the present small-scale

laboratory campaign, it is possible to observe the same findings of the large-scale experiments performed by Oumeraci et al. (1993) and Bullock et al. (2007). Indeed, the *surging* wave pressure signals (a) show all the characteristics of a *high-aeration impact load*: the ratio between the maximum peak and the quasi-hydrostatic peak, $p_{max}/p_{h,q}$, is greater than 2.5 for all the pressure transducers and the signals are characterized by strong oscillations due to the huge air content inside the wave front, with a sub-atmospheric peak after the first expansion phase. The second impact (b) shows the shape characteristic of the *slightly breaking* impact (*plunging* wave): in this case, the ratio $p_{max}/p_{h,q}$ varies between 1 and 2.5 as for the large-scale experiments (Oumeraci et al., 1993; Bullock et al., 2007) and the pressure signal is smoother and the frequency of the oscillations is lower due to the smaller air content. The last impact (c) is classified as *broken*, with a ratio of $p_{max}/p_{h,q} \approx 1$ and oscillations denoting a huge presence of air, which in this case is in form of bubbles due to the earlier breaking process. This latter impact presents on average a frequency of occurrence of ~17%, which becomes close to ≈100% in case of $A_c>0$, when the wave breaking always occurs along the dike slope during the wave run-up phase. Though all the tests with $A_c=0$ present both plunging and surging breaker types, the most frequent impacts correspond to *plunging* waves (≈85%), especially in case of $cot\alpha=4$ (>90%), when $\xi_{m-1,0}$=1.23-1.94. The *surging* breaker type is more frequent (≈13%) in case of $cot\alpha=2$, with values of $\xi_{m-1,0}$=2.38-4.03.

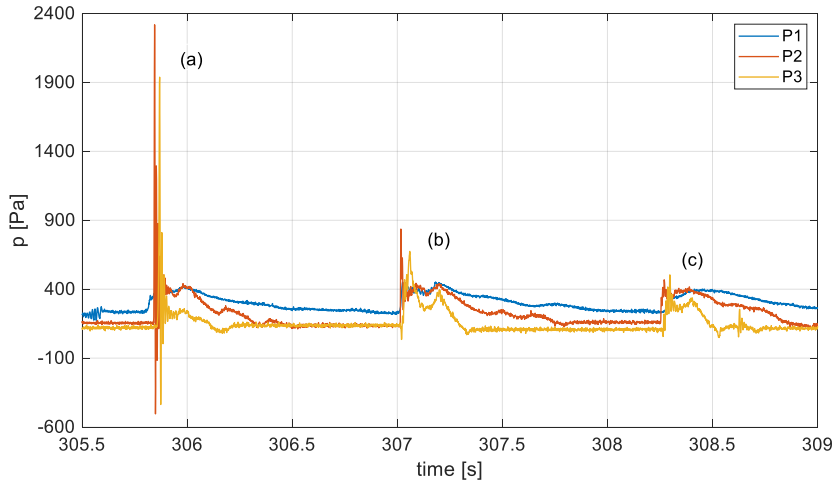

Figure 5. Time-domain pressure signals related to: a) a surging breaker, b) a plunging breaker, and c) a broken wave type.

Geometric and hydraulic parameter effects on the pressure profiles

This section presents the pressure vertical profiles, for both *breaking* and *non-breaking* waves. Note that the adjectives "breaking" and "non-breaking" are here used to refer to the *target* wave conditions of the tests based on the *target* values of $\xi_{m-1,0}$ respectively < and >2, and not to the characteristics of the single wave impacts. Indeed, as already specified and as shown in Figure 5, each test presents both breaking and non-breaking waves. Into specific, the analysis shows the effects of the geometric parameters, combined with the wave conditions, on the vertical pressure distributions. The reference value is the statistical pressure p_{250}, which is the average of the highest N/250 impact events, where N is the number of waves of the test time series. It is widely used in the literature, being more representative of the wave impact dynamic with respect to the maximum pressure. Therefore, for each tested configuration the vertical profiles were reconstructed by computing the dimensionless values of $p_{250}/(\rho g H_s)$ in correspondence of the pressure transducers installed along the crown wall, where ρ is the water density, g the gravitational acceleration and H_s the significant wave height.

Plunging and broken waves

Figure 6 shows an example of the vertical non-dimensional pressure $p_{250}/(\rho g H_s)$ distributions for the *breaking* configuration with $cot\alpha=4$ and h_w=0.05 m, presenting in most cases *plunging* or *broken* waves. Each panel shows the effects of the G_c variation (0.15 and 0.30 m in light and dark green, respectively) and of the introduction of the parapet (dashed line instead of solid line). Starting from the benchmark case (Figure 6, panel a), corresponding to the case of H_s=0.05 m, $A_c/H_s=0$, $s_{m-1,0}$=3%, G_c=0.15, no parapet,

the other panels highlight the effect of the variation of i) A_c/H_s from 0 (panel a) to 0.5 (panel b), ii) $s_{m-1.0}$ from 3% (panel a) to 4% (panel c) and iii) H_s from 0.05 m (panel a) to 0.06 m (panel d).

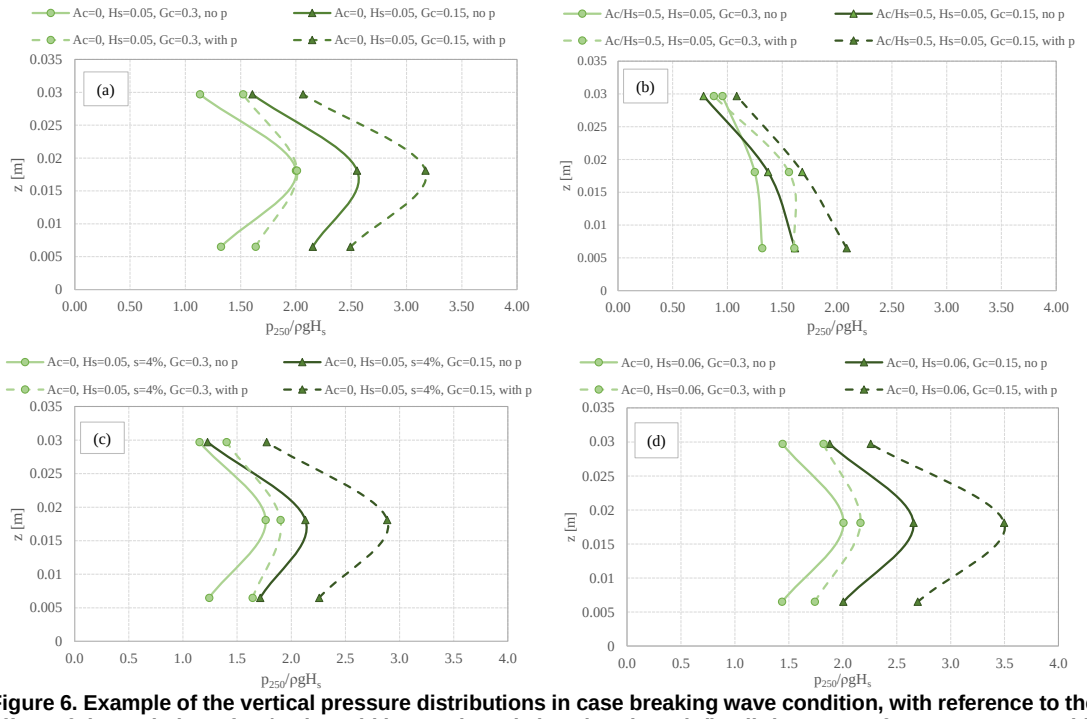

Figure 6. Example of the vertical pressure distributions in case breaking wave condition, with reference to the effect of the variation of A_c/H_s (panel b), $s_{m-1.0}$ (panel c) and H_s (panel d). All the tests refer to structures with $cot\alpha$=4 and h_w=0.05 m.

By increasing the crest width G_c (light green lines in Figure 6), there is a strong reduction of the wave pressure along the crown (≈ 60-70%, on average), which is more pronounced if combined with the parapet (dashed lines in Figure 6). However, the inclusion of the parapet does not induce a systematic effect on the pressure trend, as it is highlighted by the average non-dimensional values of $p_{250}/(\rho g H_s)$ in case of crown walls (1.53, 1.80 and 1.20 at P1, P2, P3, respectively) and wall with parapet (1.60, 1.78, 1.20). The variation of the crest freeboard A_c/H_s strongly affects the entity of the wave loads. Indeed, the emerged cases (A_c/H_s = 0.5) show a reduction of the values of $p_{250}/(\rho g H_s)$ in the range of 15-100%, with respect to the crest at the still water level (A_c/H_s=0). Furthermore, in emerged conditions (A_c/H_s=0.5, see panel b in Figure 6), the shape of the vertical distribution presents a triangular distribution, recalling a hydrostatic-shape distribution. This is due to the fact that the number of wave impacts decreases from P1 to P3, lowering the values of $p_{250}/(\rho g H_s)$ towards the upper part of the crown wall (both with and without the parapet). The wave steepness $s_{m-1,0}$ and the wave height H_s seems to play pure scale effects. Indeed, higher values of $s_{m-1,0}$ and of H_s induces a reduction and an increase of the wave loads reduction (Figure 6 panel a vs. panel c), respectively.

Surging waves

Figure 7 shows representative vertical profiles of $p_{250}/(\rho g H_s)$ for the *non-breaking* configuration, with h_w=0.04 m and $cot\alpha$=2, presenting more frequently *surging* waves (≈13%) than other configurations. In each panel of Figure 7, the values of H_s and $s_{m-1,0}$ and A_c/H_s are kept constant, showing the effects of the variation of G_c (0.15 and 0.30 m in light and dark orange shading, respectively) and the presence of the parapet (dashed line instead of continuous). The 2 panels highlight the effect of increasing A_c/H_s from 0 (panel a) to 0.5 (panel b). The values of $s_{m-1,0}$ and H_s (which are respectively equal to 0.03 and 0.05 m in both the panels) are not considered because there is no relevant difference with respect to the case of *plunging* waves (see Figure 6), while G_c does not play a systematic role in the reduction of the wave loads, differently from the previous cases. However, the main difference between the *plunging* and *surging* wave conditions is represented by the effect of parapet that strongly increases in the latter case the wave loads acting along the wall (50-70% on average, reaching and exceeding in some cases of the 100%). The average non-dimensional values of $p_{250}/(\rho g H_s)$ for P1, P2 and P3, computed on the whole

dataset of tests with *cotα*=2, are 1.79, 2.16 and 1.47 in case of simple crown walls, and 2.00, 2.56 and 1.87 when the parapet is included. The same phenomenon was observed by comparing the loads in case of recurved seawalls and vertical walls (Kortenhaus et al., 2003; Castellino et al., 2018), where the difference between the peak pressures in the 2 cases is up to 2 times for *breaking* waves and even 10 times for *non-breaking* waves.

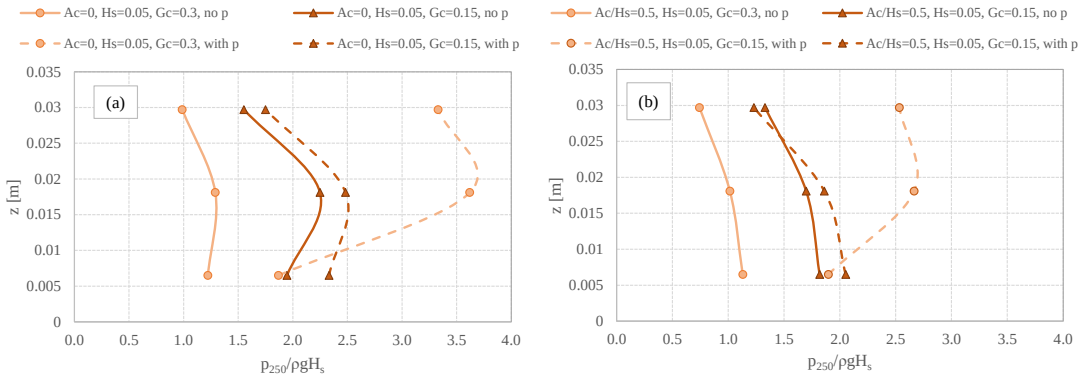

Figure 7. Example of the vertical pressure distributions in case non-breaking wave condition, with reference to the effect of the variation of A_c/H_s (panel b). All the tests refer to structures with $cot\alpha$=2 and h_w=0.04 m.

NUMERICAL MODELLING RESULTS

This Section presents the results obtained by means of the numerical investigation performed on a sub-set of the laboratory experiments. Firstly, the model was validated based on the average overtopping discharge rates q and on the reflection coefficients K_r, to assess its capability of reproducing the laboratory tests. Secondly, the numerical model was adopted to analyze the forces and the air content associated to the wave impacts.

Model calibration

Table 5 reports the characteristics of the tests reproduced by means of the numerical model. Specifically, it reports the ID that identifies the tested case, the freeboard of the crest width A_c, the freeboard of the crown wall R_c, the values of cotα, the significant wave height H_s, the peak and the spectral period T_p and $T_{m-1.0}$, the wave length $L_{m-1.0}$ and the relative freeboard of the crown wall R_c/H_s. The calibration subset was selected to account for the variation of the wave steepness $s_{m-1,0}$, the significant wave height H_s and the freeboard condition of the crest. Figure 8 and Figure 9 show the comparison among the laboratory (subscript *lab*) and the numerical (subscript *mod*) results in terms of the average overtopping discharge rates q and of the reflection coefficients K_r, respectively. The values of q_{mod} show a good agreement with the laboratory results (Figure 8), despite of the different methodologies used to quantify the average overtopping discharge rates. Indeed, the values of q_{lab} are reconstructed from the overtopping volumes, while in the numerical model the horizontal velocity components, combined with the VOF values, are integrated along the vertical gauge, placed at the rear side of the crown wall (see Figure 3). The values of K_r are slightly underestimated by the numerical model (see Figure 9). Eventually, to quantify the reliability of the numerical model, 3 different errors were computed, i.e. the *relative error* (Eq. 1), the *RMSE* (Eq. 2) and the *Wilmott index* (Eq. 3). The performance is high when the first 2 parameters go to 0, while the third goes to 1. The results are shown in Table 6, for both the values of q and K_r.

Table 5. Main characteristics of the sub-set of the tests carried-out by means of the numerical model.

ID	A_c	R_c	$cot\alpha$	$H_{s,target}$	$T_{p,target}$	$T_{m-1.0}$	$L_{m-1.0}$	R_c/H_s
A00H05s3G30c4W4	0.0	0.040	4.00	0.05	1.21	1.10	2.28	0.80
A00H05s4G30c4W4	0.0	0.040	4.00	0.05	1.02	0.93	1.63	0.80
A00H06s3G30c4W4	0.0	0.040	4.00	0.06	1.38	1.25	2.97	0.67
A05H05s3G30c4W4	0.5	0.065	4.00	0.05	1.21	1.10	2.28	1.30
A00H05s3G30c2W4	0.0	0.040	2.00	0.05	1.21	1.10	2.28	0.80
A00H05s4G30c2W4	0.0	0.040	2.00	0.05	1.02	0.93	1.63	0.80
A00H06s3G30c2W4	0.0	0.040	2.00	0.06	1.38	1.25	1.97	0.67
A05H05s3G30c2W4	0.5	0.065	2.00	0.05	1.21	1.10	1.65	1.30

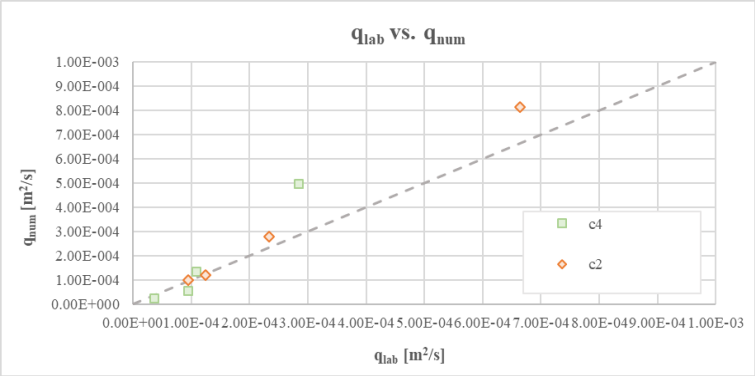

Figure 8. Comparison between the laboratory and the numerical average overtopping discharge rates q [m²/s].

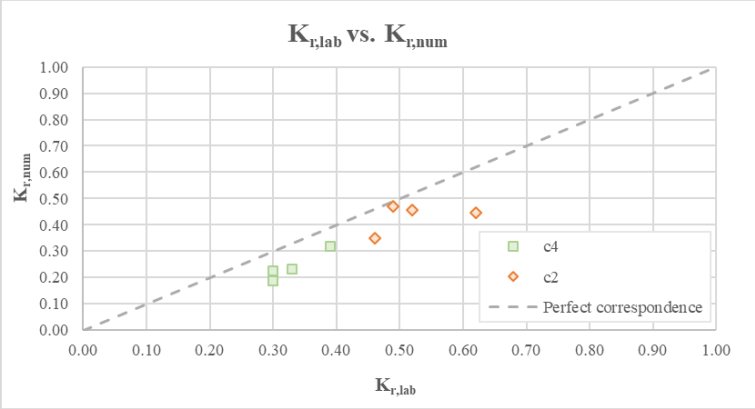

Figure 9. Comparison between the laboratory and the numerical reflection coefficients K_r [/].

$$\delta_x = \frac{y_{lab,j} - y_{mod,j}}{y_{lab,j}} \quad (1)$$

$$\mathrm{RMSE} = \sqrt{\frac{1}{N}\sum_{J=1}^{n}\left(y_{lab,j} - y_{mod,j}\right)^2} \quad (2)$$

$$WI = 1 - \frac{\sum_{j=1}^{N}\left(y_{lab,j} - y_{mod,j}\right)^2}{\sum_{j=1}^{N}\left[\left|y_{lab,j} - \overline{y_{lab}}\right| + \left|y_{mod} - \overline{y_{lab}}\right|\right]^2} \quad (3)$$

Table 6. Relative error, RMSE and Wilmott index to quantify the reliability of the numerical model in predicting the experimental values of q and K_r.

Errors	Relative error	RMSE	Wilmott index
q	9.21%	0.00009	0.95
K_r	-16.40%	0.09	0.90

Numerical analysis of the wave impacts

The numerical model was adopted to investigate the wave impact dynamics. As for the pressures, the hydrodynamic forces F were treated as stochastic values, and the statistical values of F_{250} were computed as the average force value of the highest $N/250$ impact events, where N is the number of waves of the tested time series. Figure 10 shows the comparison between the experimental and the numerical values of $F_{250}/\rho g R_c^2$. The numerical model slightly overestimates the forces measured during the

laboratory campaign, for both *breaking* and the *non-breaking* waves. Specifically, the higher are the forces, the higher is the discrepancy.

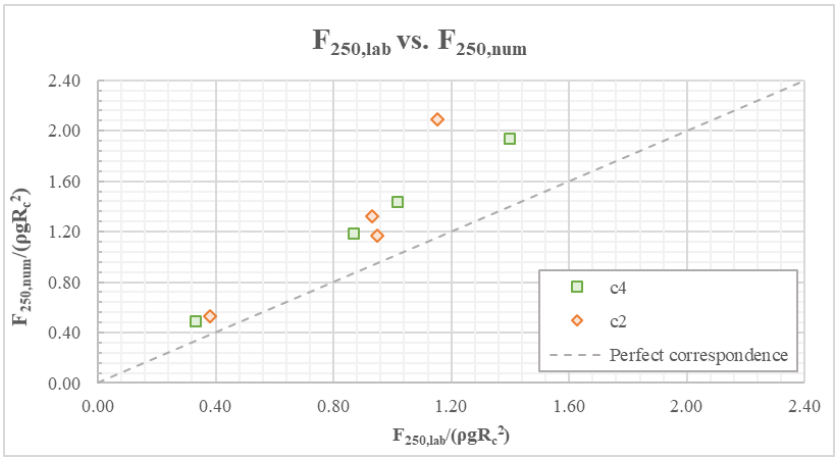

Figure 10. Comparison between the laboratory and the numerical statistical non-dimensional values of $F_{250}/\rho gRc^2$.

Although several studies are available for the analysis of wave impacts against rubble mound crown walls (a.o. Franco et al., 2018; Jacobsen et al., 2018), the literature related to crown walls placed on top of smooth dikes is very limited. Van Doorslaer et al. (2017) was the first to propose a design formula to predict the wave forces, under irregular wave series, based on *non-breaking* waves only. Such formula considers the non-dimensional $F_{250}/\rho gR_c^2$, predicting an exponential decreasing trend of the wave forces with the relative freeboard R_c/H_{m0} (Eq. 4), where b is equal to -2.02 and -2.4 for small-scale (1:10, 1:15) and large-scale (1:6) tests, respectively. Figure 11 shows the comparison of the numerical values of $F_{250}/\rho gR_c^2$, with the formula by Van Dooslaer et al. (2017), presented in Eq. 4. The pressure signal analysis highlighted that the most frequent impact in the present investigation (80-86%) is the *slightly breaking* impact, i.e. a plunging wave that represents a transition phase between the surging (pure *non-breaking*) and the broken wave (pure *breaking*). The numerical forces show a good agreement with the formula developed by Van Dooslaer et al. (2017), despite of the different model scale.

$$\frac{F_{250}}{\rho g R_c^2} = 7.8 \cdot exp\left(b \cdot \frac{R_c}{H_{m0}}\right) \tag{4}$$

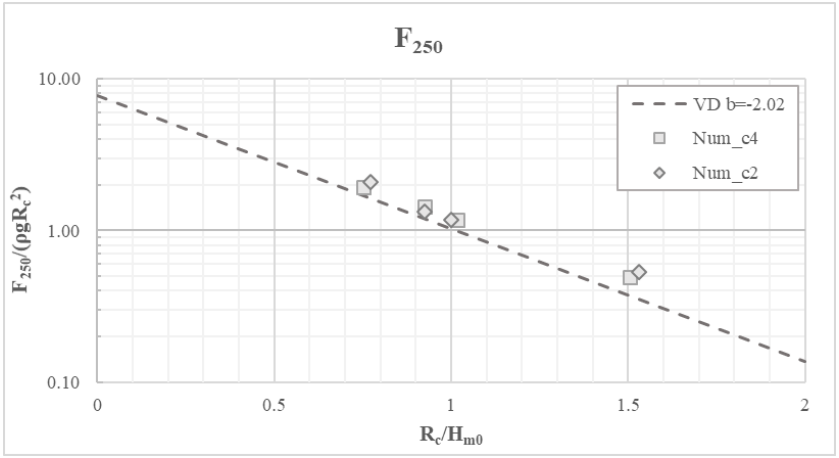

Figure 11. Comparison of both the laboratory and numerical values statistical forces with Eq. Errore. L'origine riferimento non è stata trovata.**), where b=-2.02.**

The numerical model was used to quantify the air content along the crown wall, in correspondence of the virtual pressure transducers (Figure 3). The required outputs are related to the Volume of Fluid (VOF) values, which varies from 0 (air) to 1 (water). Table 7 reports the percentage of the air content measured during the numerical simulations $VOF_{air,\%}$. As expected, the highest percentages were registered towards the top of the crown wall, which is rarely reached by the wave front. Indeed, lower values are measured only for the case of H_s=0.06 m that represents the highest simulated wave height. The most interesting aspect can be observed by comparing the zero-freeboard case R00H05s3G30c4W4 with the corresponding one characterized by an emerged freeboard crest, i.e. R05H05s3G30c4W4. In fact, even if the still water level is lower than the freeboard crest, the incoming waves always hit the crown wall, even if with lower intensity. Therefore, the highest values of $VOF_{air,\%}$, registered in the lower part of the crown wall, are due to the presence of air bubbles, caused by the early breaking process. The same results can be observed for the tests characterized by a $cot\alpha$=2 (Table 7).

Table 7. Percentage of the air content measured during the numerical simulations $VOF_{air,\%}$, in correspondence of the virtual pressure transducers.

ID	**1** (0.005m)	**2** (0.01m)	**3** (0.015m)	**4** (0.02m)	**5** (0.025m)	**6** (0.03m)	**7** (0.035m)	**8** (0.04m)
R00H05s3G30c4W4	5%	14%	44%	54%	69%	79%	85%	87%
R00H05s**4**G30c4W4	5%	12%	46%	58%	75%	84%	90%	92%
R00H0**6**s3G30c4W4	6%	11%	36%	46%	60%	70%	77%	80%
R0**5**H05s3G30c4W4	21%	30%	78%	86%	89%	92%	95%	95%
R00H05s3G30c2W4	3%	8%	42%	53%	68%	78%	83%	85%
R00H05s**4**G30c2W4	4%	8%	44%	56%	72%	82%	88%	90%
R00H0**6**s3G30c2W4	5%	10%	40%	49%	63%	72%	79%	82%
R0**5**H05s3G30c2W4	15%	24%	78%	86%	90%	93%	96%	97%

CONCLUSIONS

A new small-scale laboratory campaign, involving 128 tests, was performed at the Hydraulic Laboratory of Bologna. The experimental analysis aimed to analyze the wave overtopping and the wave impacts at dikes with crown walls and parapets. Different structure configurations were tested under irregular wave attacks, including both *breaking* ($\xi_{m-1,0}$≈1.23-2) and *non-breaking* waves ($\xi_{m-1,0}$≈1.23-2). The tested configurations included different dike slopes, crest widths and freeboards, crown wall heights with or without a top parapet.

The specific objective of the investigation was to perform a parametric analysis of the effects of the structure geometrical parameters on the wave impacts acting on the crown walls. The preliminary analysis of the image frames and of the pressure signals allowed to associate the tested configurations and the breaker types. As for large-scale experiments (Oumeraci, et al., 1993; Bullock et al., 2007; Plumerault et al., 2012), the magnitude of the impact pressure and the shape of its signal is strongly dependent on the breaker type and the amount of air pockets entrapped. Indeed, the most violent impacts observed are associated to the *non-breaking* wave conditions, characterized by the presence of small air pocket. In case of *breaking*/*broken* waves, the crest width G_c significantly contributes to reduce the magnitude of p_{250}, up to 60-70%. Therefore, the increase of the crest width might represent an effective solution to reduce the enhanced loads due to the parapet inclusion on the top the crown wall. In case of *non-breaking* waves, the introduction of the parapet induces a severe increase of the values p_{250}, i.e. 50-70% on average; while the effect of G_c is negligible. Therefore, the inclusion of parapet in case of structures subjected to surging waves is not recommended.

A numerical investigation was performed on a sub-set of the experimental tests. The model calibration was performed based on the overtopping discharge rates q and the reflection coefficients K_r obtained from the experimental campaign. The accuracy of the model was assessed by means of 3 error indices, i.e. the *relative error*, the *RMSE* and the *Wilmott index*. For the values of q the *relative error*, the *RMSE* and the *Wilmott index* are -9.21%, 0.0009 and 0.95, while for K_r, -16.40%, 0.09 and 0,90, respectively. The statistical values of F_{250} are slightly overestimated by the numerical model. However, considering that the pressure signal analysis highlighted the slightly breaking impact as the most frequent in the present investigation (80-86%), the numerical results were compared with the formula developed by Van Dooslaer et al. (2017), tuned on similar structures under *non-breaking* wave conditions. The analysis performed shows a good agreement between the theoretical formulation and the numerical results, despite the different model scales. The numerical model was used to qualitatively assess the air content $VOF_{air\%}$ in correspondence of the virtual pressure transducers. As expected, the top of the crown

wall registered the highest values of $VOF_{air\%}$ because less frequently reached by the waves. Indeed, these values resulted to be lower in case of H_s=0.06 m, the highest tested significant wave height. The tests characterized by an emerged freeboard crest shows high values of $VOF_{air\%}$ at the base of the crown wall, with respect to the correspondent cases with the crests at the still water level. This result indicates a huge presence of air bubbles in the wave front, due to the earlier breaking process that occurs along the offshore slope. Further research will focus on the validation of these data with the support of image analysis to quantify the air content according to the breaker type and its direct consequence on the magnitude of the pressures and so the forces.

ACKNOWLEDGMENTS

The support of the European Union's Horizon 2020 research and innovation program under grant agreement 700699 BRIGAID ("BRIdging the GAp for Innovations in Disaster resilience") is gratefully acknowledged.

REFERENCES

Bullock, G.N., Obhrai, C., Peregrine, D.H. and Bredmose, H. (2007). Violent breaking wave impacts. Part 1: Results from large-scale regular wave tests on vertical and sloping walls, Coastal Engineering, 54, 602-617.

Burcharth, H.F., Lykke Andersen, T., Lara, J.L. (2018). Upgrade of coastal defence structures against increased loadings caused by climate change: a first methodological approach, Coastal Engineering 87, 112-121.

Castellino M., Sammarco P., Romano A., Martinelli L., Ruol P., Franco L. and De Girolamo, P. 2018. Large impulsive forces on recurved parapets under non-breaking waves. A numerical study. Coastal Engineering 136, 1–15.

De Finis, S., Romano, A., & Bellotti, G. (2020). Numerical and laboratory analysis of post-overtopping wave impacts on a storm wall for a dike-promenade structure. Coastal Engineering, 155, 103598.

Formentin, S.M. and Zanuttigh, B., 2019. A Genetic Programming based formula for wave overtopping by crown walls and bullnoses, Coastal Engineering 152, 103529, 17 pp.

Franco, L., Belotti, G. and Cecioni, C., 2018. Physical model tests of wave overtopping and forces on breakwater crown walls, in Proceedings of 36th ICCE, Baltimore (MD), 2018.

Jacobsen, N. (2017). waves2foam manual. Deltares, The Netherlands.

Kortenhaus A., Pearson, J. Bruce, T. Allsop W., Van der Meer J., 2003. Influence of parapets and recurves on wave overtopping and wave loading of complex vertical walls. Proc. Coast. Struct. 2003, 369–381.

Liu, S., Gatin, I., Obhrai, C., Ong, M. C., & Jasak, H. (2019). CFD simulations of violent breaking wave impacts on a vertical wall using a two-phase compressible solver. Coastal Engineering, 154, 103564.

Ma, Z., H., Causon, D., M., Qian, L., Mingham, C. G., & Ferrer, P. M. (2016). Numerical investigation of air enclosed wave impacts in a depressurised tank. Ocean Engineering, 123, 15-27.

Martinelli L., Ruol P., VolpatoM., Favaretto C., Castellino M., De Girolamo, P., Franco, L., Romano A. and Sammarco, P., 2018. Experimental investigation on non-breaking wave forces and overtopping at the recurved parapets of vertical breakwaters, Coastal Engineering 141, 52–67.

Oumeraci, H., Klammer, P., & Partenscky, H. W. (1993). Classification of breaking wave loads on vertical structures. Journal of waterway, port, coastal, and ocean engineering, 119(4), 381-397.

Battjes, J. A. (1975). Surf similarity. In Coastal Engineering 1974 (pp. 466-480).

Plumerault, L.R., Astruc, D. and Maron, P. (2012). The influence of air on the impact of a plunging breaking wave on a vertical wall using a multifluid model, Coastal Engineering, 62, 62-74.

Van Doorslaer, K., De Rouck, J., Audenaert, S. and Duquet, V., 2015. Crest modifications to reduce wave overtopping of non-breaking waves over a smooth dike slope, Coastal Engineering, 101, 69–88.

Van Doorslaer, K., Romano, A., De Rouck, J., & Kortenhaus, A. (2017). Impacts on a storm wall caused by non-breaking waves overtopping a smooth dike slope. Coastal Engineering, 120, 93-111.

Zanuttigh B. and Formentin S.M. (2018). Reduction of the wave overtopping discharge at dikes in presence of crown walls with bullnoses, Proc. of XXXVI ICCE, Baltimore.

Zelt, J. A., & Skjelbreia, J. E. (1993). Estimating incident and reflected wave fields using an arbitrary number of wave gauges. In Coastal Engineering 1992 (pp. 777-789).